Entrapment of polysulfides by phosphorene modified separator for lithium-sulfur batteries

Jie Sun,[1] Yongming Sun,[1] Mauro Pasta,[1] Guangmin Zhou,[1] Yuzhang Li,[1] Wei Liu,[1] Feng Xiong,[1] Yi Cui*[1,2]

[1]*Department of Materials Science and Engineering, Stanford University, Stanford, California 94305, USA,* [2]*Stanford Institute for Materials and Energy Sciences, SLAC National Accelerator Laboratory, 2575 Sand Hill Road, Menlo Park, California 94025, USA.*

Abstract

Despite the high theoretical specific energy density and low cost, the practical application of lithium-sulfur batteries is still hindered by their poor cycle life and low power capability. Two critical problems that lead to the quick capacity decay upon cycling are the dissolution of the soluble intermediate polysulfide species (lithium polysulfides, Li_2S_x, $3 \leqslant x \leqslant 8$) into the electrolyte and the "shuttle effect" caused by these soluble species. Physical and chemical trapping of sulfur and polysulfides within the electrode have been extensively investigated, however, only a few studies focused on the entrapment of polysulfides beyond the electrode design (e.g., electrolytes and functional separators). In this work, a bifunctional separator, consisting of a phosphorene layer deposited on a commercial Celgard polypropylene separator, was designed and fabricated to overcome the challenges associated to polysulfide diffusion in lithium-sulfur batteries. We demonstrated the following benefits: (i) The phosphorene layer on the separator strongly binds to various sulfur species thus preventing the diffusion of the soluble polysulfides to the anode side. (ii) Phosphorene possesses high electron conductivity and Li ion diffusivity, so that it can "activate" the trapped sulfur species thus enabling high capacity retention and enhanced long-term cyclability. High discharge capacity (930 mAh g^{-1}) and capacity retention (86%, after 100 cycles) were achieved for a cathode with a high sulfur content (80 wt%).

*Corresponding author: yicui@stanford.edu.

TOC graphic

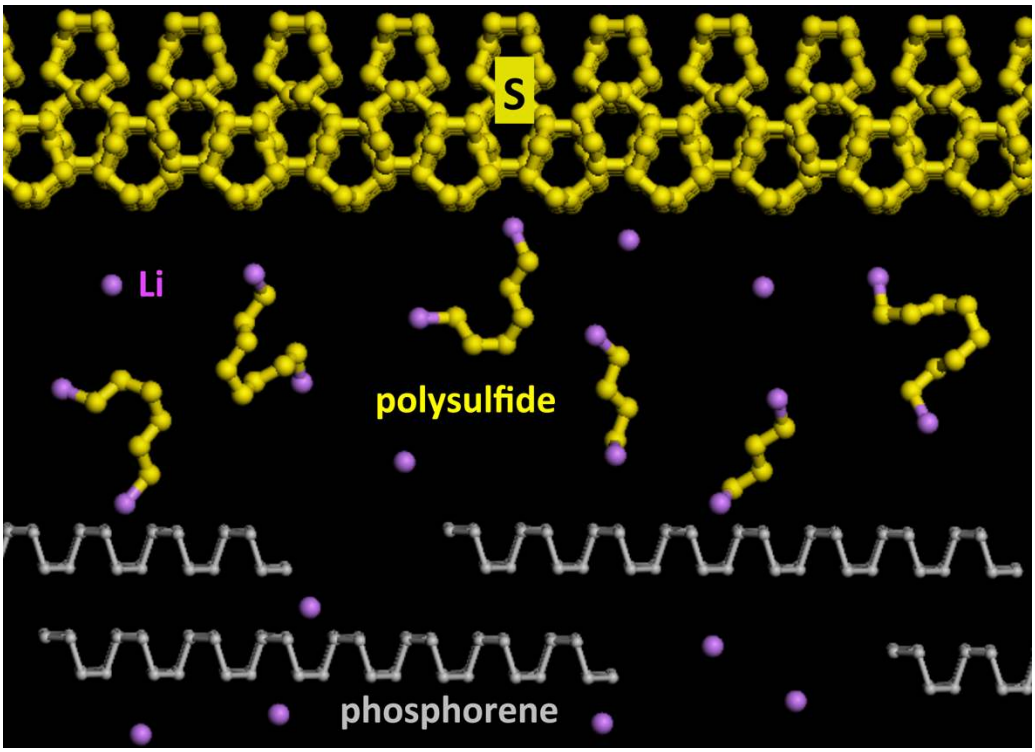

With the increasing demand for high capacity energy storage systems, a considerable amount of effort has recently been focused on the development of the lithium–sulfur (Li–S) battery due to its high theoretical energy density (2567 W h kg^{-1}) and the abundance, non-toxicity and low cost of sulfur.[1–3] Despite the great promise, successful implementation of the Li-S battery is still hindered by its short cycle life and limited power density. Several problems need be addressed to enable its practical application: i) The low electrical conductivity of sulfur species, which leads to high overpotentials and low utilization of active materials.[4–6] ii) The diffusion of soluble intermediate polysulfide species into the electrolyte, which causes irreversible loss of active material, low coulombic efficiency, short cycle life and increases the device impedance over time.[7,8] iii) The large volume change of sulfur cathodes during the charge and discharge processes (up to 80%), which induces stress in the electrode and undermines its structural integrity, leading to the loss of electrical contact with the conductive additives and the detachment from the current collector.[9,10]

To address these issues, extensive research has been devoted to engineering the electrode structure and composition to increase the electrical conductivity and to prevent the polysulfide dissolution by physically and/or chemically trapping the sulfur species within the electrodes. To date, several important strategies for advanced electrode design have been explored such as nanoporous carbon-sulfur composites,[11,12] conductive polymer-sulfur composites,[13] as well as metal oxide and sulfide coating[14–16]. Moreover, various routes for the physical trapping of soluble polysulfides beyond the electrode have been explored, including the insertion of a microporous carbon paper between cathode and separator[17,18] and the modification of separators with a carbon coating layer.[19–21] Although carbon materials have shown promise as sulfur-entrapping host structures,[11,12,17–20] their weak interaction with the polar Li_2S_x undermines their application as polysulfide traps.[12–14]

Here we introduce a new Li-S battery functional separator obtained by depositing a sulfur-capturing 2D phosphorene layer onto a Celgard, commercial polypropylene separator. We show how the combination of both the physical and chemical bonding between polysulfides and phosphorene results in superior polysulfide-capturing properties and consequently a superior capacity retention upon cycling. An in-depth *in-situ* and *ex-situ* characterization is carried out to investigate the nature of the polysulfide-phosphorene interaction and compare it to graphene and other polar polymers [12,13].

2D phosphorene is defined as a monolayer or few layers (< 10 layers) of phosphorene stacked in puckered sub-planes through weak interlayer van der Waals interactions. In a phosphorene monolayer, each P atom is bonded with two adjacent atoms lying in the same plane and with a third P atom from a different plane.[22-24] It has been successfully isolated from black phosphorus (BP), the most thermodynamically stable allotrope of phosphorous,[22] via liquid exfoliation [23] or sticky-tape

cleavage[24]. In terms of appearance, properties and structure, BP closely resembles graphite: it is black, flaky and a good electrical conductor (~300 S m^{-1}).[22] Moreover, the Li^+ diffusion constant within a phosphorene monolayer (zigzag direction) is estimated to be 10^4 times faster than that on graphene at room temperature.[25] In addition, the bonding energies between phosphorene and S containing species ranges from 285 to 442 kJ/mol, slightly lower than the 485 kJ/mol of a P—P bond.[26] This suggests that phosphorene can chemically interact with the polysulfides without structurally damaging the phosphorene backbone. Once bonded, the good electrical conductivity and the fast Li-ion diffusion properties of the phosphorene layer can "reactivate" the polysulfide species, thus minimizing the capacity loss associated with the active material dissolution.

Figure 1a shows a schematic representation of a coin cell with a conventional and phosphorene-coated separator. The phosphorene-coated side, facing the sulfur-based cathode electrode, intercepts and binds the polysulfides preventing their diffusion through the polypropylene separator (**Figure 1b**). The vacuum filtration deposition process (**Figure 1c-d**) results in an excellent adhesion of phosphorene to the commercial separator, as demonstrated by the folding/unfolding test in **Figures 1e-f**. Scanning electron microscopy (SEM) images of the Celgard polyethylene separator (Supplementary, **Figure S1**) show its typical nanoporous (~100 nm pore diameter) structure. After the 2D phosphorene deposition, a uniform and dense layer of phosphorene nanoflakes (~0.4 mg cm^{-2}) forms on the surface of the separator, covering the nanopores (**Figures 1g-h**). A detailed characterization of the phosphorene nanoflakes is reported in the Supplementary Information (**Figures S2 and S4)**.

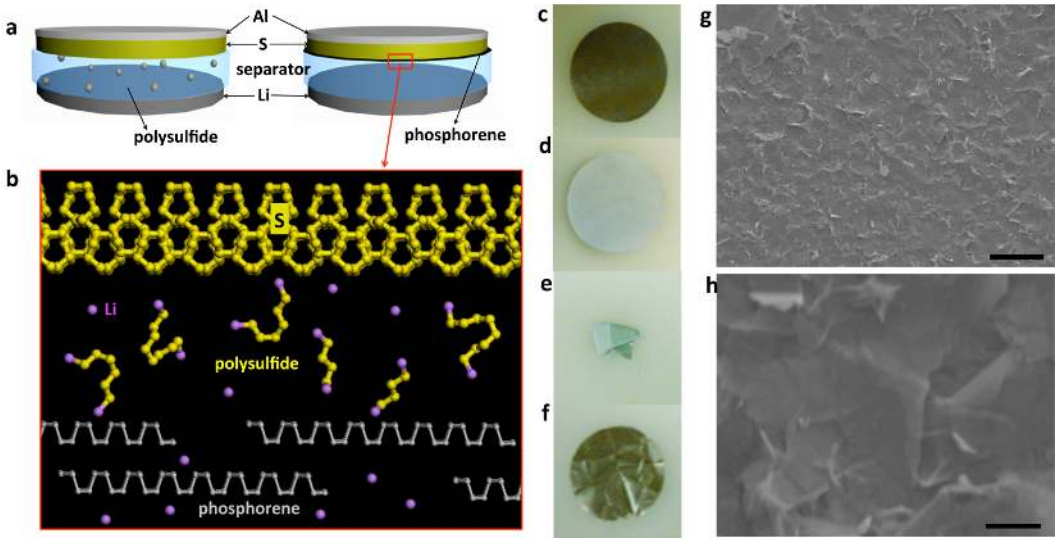

Figure 1. (a) Schematic cell configuration of the Li−S cell employing a commercial separator (left) and the phosphorene-coated separator (right). (b) Operating principle of the phosphorene coating layer in

Li-S battery. Photographs of the as-prepared phosphorene-coated separator: (c) cathode-facing side (d) anode-facing side (e) folded and (f) unfolded. (g) SEM image of the as-prepared phosphorene-coated separator. (h) High magnification SEM image of the as-prepared phosphorene-coated separator. The scale bars in g and h are 10 μm and 1 μm, respectively.

In-situ Raman spectroscopy was employed in order to characterize the transition from S_8 to Li_2S during cycling. A prototype Li–S cell for in-situ Raman characterization is shown in **Figure S5** in which a sandwich structure composed of a sulfur cathode coated on aluminum foil, a phosphorene-coated separator and a lithium metal on copper foil anode was assembled into a transparent pouch cell. The anode and separator were punched with a circular hole in the center to expose the cathode to the incident laser beam. As shown in **Figure 2a**, the Raman spectra were recorded at five charge states: at open circuit voltage (OCV) 2.42 V (A), 2.10 V (B), 1.70 V (C), 2.39 V (D) and 2.60 V (E) respectively during the first discharge/charge cycle. **Figure 2b** shows the typical Raman spectra collected from the cathode at different potentials/charge states. It reveals the evolution of the chemical composition on the phosphorene-modified separator surface. At the 2.42 V (A), the peaks at 218 cm^{-1} and 470 cm^{-1} can be assigned to those of solid sulfur (S_8).[27] After discharging the cell to 2.1 V (B), the typical features of polysulfides (Li_2S_x, x = 3–8)[27,28] can be observed. At 1.7 V (C), the Raman spectrum shows the presence of Li_2S and Li_2S_2 [27]. After recharging the cell to 2.39 V (D), the modes of the Li_2S and Li_2S_2 species disappear and only the polysudfides signals can be observed. Further charging to 2.6 V (E), it results in the conversion of polysulfides into S_8.

In order to investigate the efficacy of the phosphorene coating layer for trapping the polysulfides, we performed in-situ Raman mapping measurements. The cathode was punched with a circular hole in the center to expose the phosphorene-coated side of the separator to the incident laser beam (**Figure 2c** and **Figure S6**). Raman mapping measurements were recorded at five charge states corresponding to points A to E in **Figure 2a.** According to the evolution of the sulfur species during the lithiation and delithiation processes, Raman mapping images were collected using different frequency ranges in **Figure 2e-i**, corresponding to the red square region in the optical microscope image in **Figure 2d**. **Figure 2e** collected at the OCV (point A) with the frequency range 213-227 cm^{-1}, shows no dissolution of the starting material, S_8. At point B (2.1 V), a bright yellow spot appears in **Figure 2f**, which was collected in the range of 390-403 cm^{-1} and was attributed to the presence of polysulfides. When the cell was discharged to 1.7 V (point C), the bright spot was recorded between 370 cm^{-1} and 385 cm^{-1} and corresponds to the formation of Li_2S and Li_2S_2 (**Figure 2g**). When charging the cell to 2.39 V (D) and 2.6 V (E), the bright spot was converted into polysulfides (**Figure 2h**) and S_8 (**Figure 2i**). It is

interesting to notice that going from (B) to (E), the distance between the big spot and the smaller one on top was almost unchanged, indicating that the phosphorene coating layer can effectively anchor the various sulfur species thus preventing the diffusion of the polysulfide anions. Moreover, its chemical evolution indicates that sulfur species bonded to the phosphorene layer are electrochemically active.

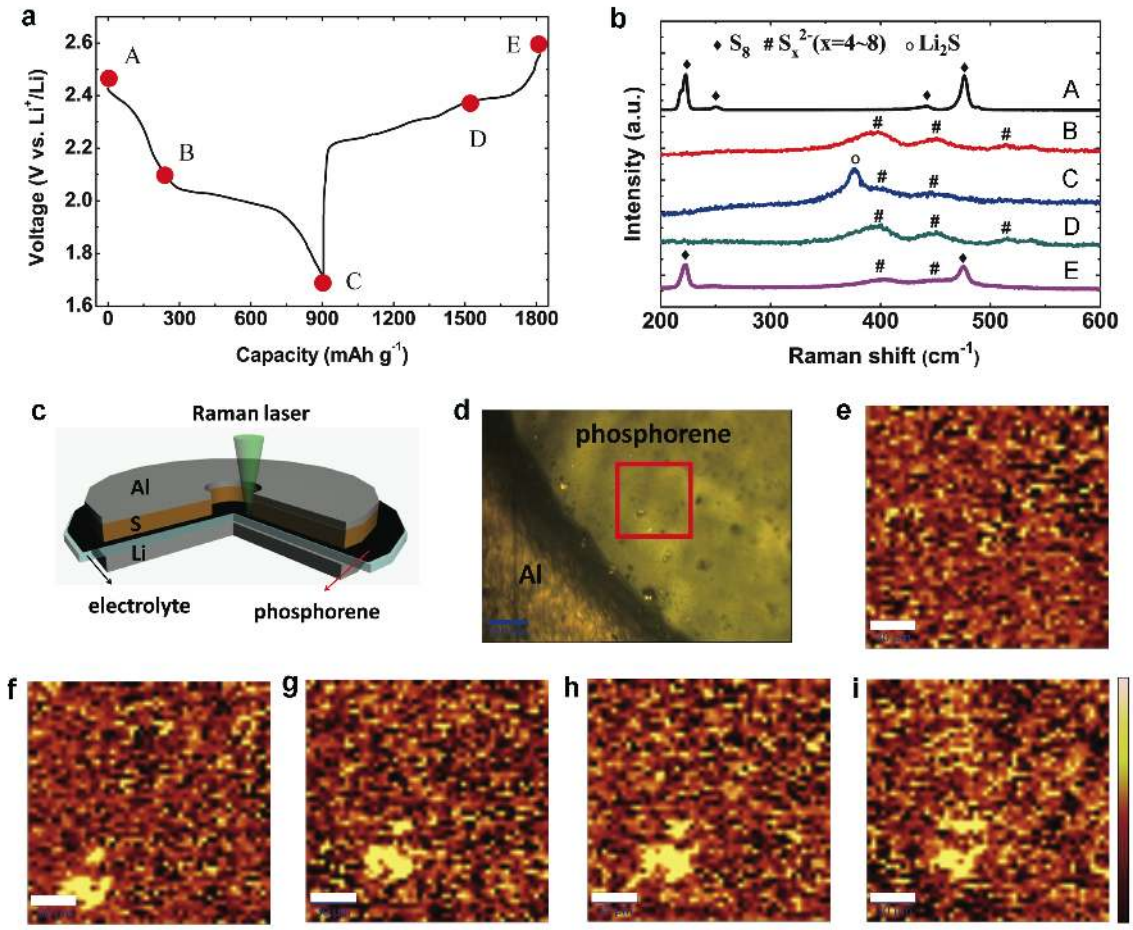

Figure 2. (a) First galvanostatic discharge–charge curves of lithium-sulfur cell. (b) Corresponding typical Raman spectra of the cathode at five different potentials. (c) Schematic of the cross section of Li-S battery with phosphorene-modified separator fabricated in a transparent pouch cell. (d) Optical microscope image of the hole in the aluminum foil. The light yellow region is the coating side of the phosphorene-modified separator. The red square represents the mapping scan region. (e)-(i) *In-situ* Raman mapping of the selected area at the sub-micron scale (red square in Figure 2c) at the potentials corresponding to (A)-(E) in Figure 2a, respectively: collecting (e) in the range of 213-227 cm^{-1}; (f) in the range of 390-403 cm^{-1}; (g) in the range of 370-385 cm^{-1}; (h) in the range of 390-403 cm^{-1}; (i) in the range of 213-227 cm^{-1}. (Raman mapping scale bars, 30 μm).

In order to further investigate the interaction between phosphorene and the anchored sulfur species, ex-situ X-ray photoelectron spectroscopy (XPS) analysis was carried out. The phosphorene-coated separators retrieved from the cycled cells were washed using 1,2-dimethoxyethane to remove the LiTFSI absorbed on the surface and transferred into the XPS machine via an oxygen-free transfer chamber. **Figures 3a-c** display a series of XPS spectra of the separators at the same potentials/charge states as the Raman characterization discussed above (**Figure 2a**). At the OCV (A), only the P $2p_{3/2}$ and P $2p_{1/2}$ signals of phosphorene were recorded (129.9 and 130.7eV, respectively). At 2.1 V (B), the Li 1*s* and S 2*p* signals can be observed. Three kinds of S 2*p* signals are clearly identifiable: S-S (S $2p_{3/2}$ at 164.1 eV), S-Li (S $2p_{3/2}$ at 161.2 eV) and S-P (S $2p_{3/2}$ at 163.1 eV). According to previous reports, the presence of the S-Li bond at this voltage demonstrates the formation of polysulfides.[29] Moreover, three P-related chemical bonds are identifiable: P-P (P $2p_{3/2}$ at 129.9 eV), P-S (P $2p_{3/2}$ at 131.6 eV) and P-Li (P $2p_{3/2}$ at 128.3 eV). These results indicate that the phosphorene interacts with polysulfides *via* both a P-S and P-Li bonds.

The interaction between phosphorene and polysulfides was investigated by first-principle calculations of the bonding energy between lithium polysulfides/sulfides and the phosphorene surface, at different sulfur loadings. The molecular models of the various lithium polysulfide/sulfide species on phosphorene as well as their binding energies, are reported in **Figure 3d**. The binding energies are in the range 1.32-2.82 eV (without van der Waals interaction), and 1.86 eV～3.05 eV (with van der Waals interaction) and increase with the shortening of the Li_2S_x molecule chains (x, from 8 to 1) due to the weak torsion dystonia. All the binding energies are higher than those on a graphene layer (0.21-0.79 eV),[13] polar polymer molecules (PVP, 1.01-1.29 eV; Triton X-100, 0.66-0.85 eV)[13] and solvent (DOL/DME, 0.85 eV)[30]. A higher binding energy indicates a more energetically favorable reaction. Therefore, the calculations show how the phosphorene layer (labeled as black, in **Figure 3d**) strongly adsorb lithium polysulfide/sulfide species by binding both Li and S atoms. These results are in agreement with the XPS data. In fact, at the end of the lower plateau at 1.7 V, the S 2*p* spectrum (**Figure 3b**) exhibits an increased proportions of S-Li and the reduced S-S bond, indicating that the lithium polysulfides (Li_2S_x, x=8-4) transforms into Li_2S_2 and Li_2S. Meanwhile, the increased proportion of S-P bond in S2*p* spectrum, as well as the increased components of both P-S and P-Li peaks in P2*p* spectra (**Figure 3a**), exhibit more P-S and P-Li bonds formed at the surface of phosphorene.

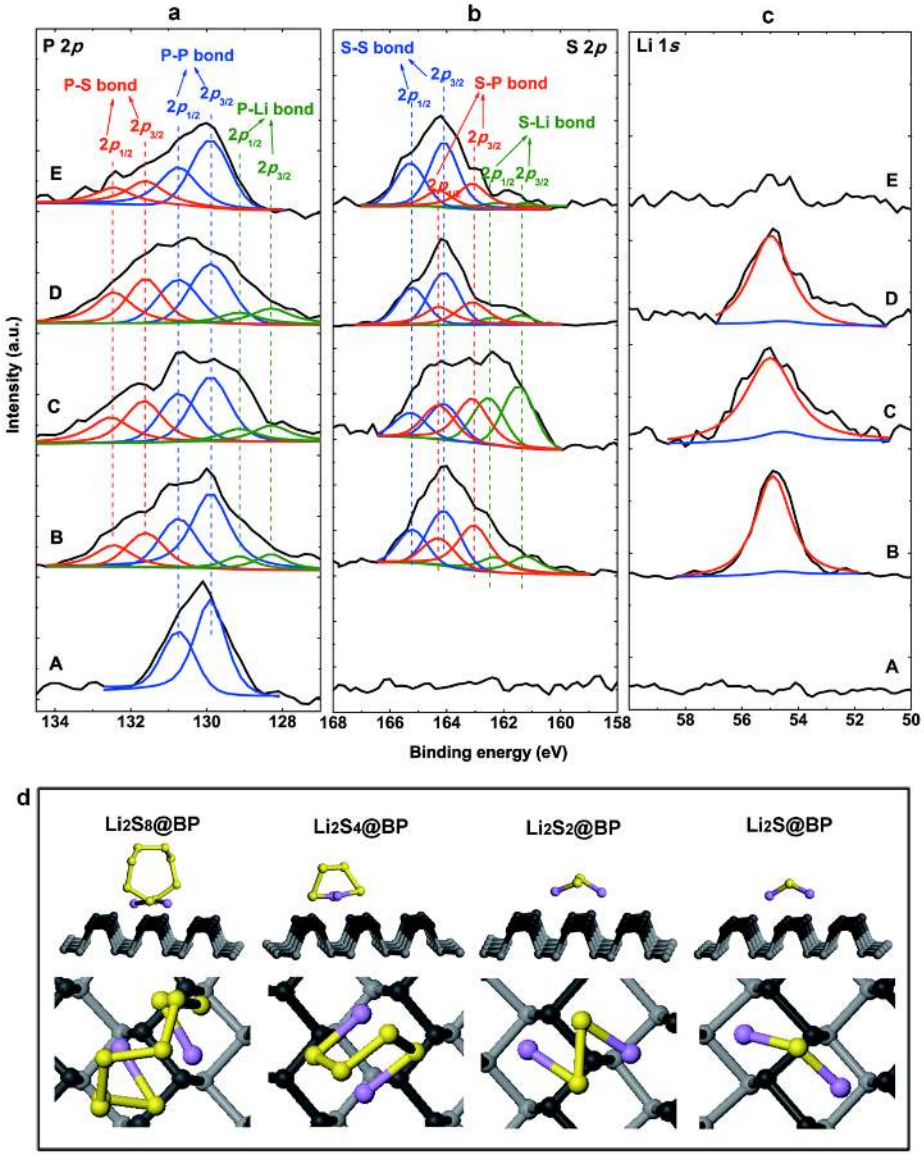

Figure 3 | XPS measurements of cycled interlayers and theoretical calculation of molecular binding. (a) P 2*p*, (b) S 2*p* and (c) Li 1*s* XPS spectra of the phosphorene-modified separators with various depth of discharge and charge at OCV (~2.4 V), 2.1 V, 1.7 V, 2.39 V and 2.6 V, respectively, according to the first discharge/charge curves of Li-S cell (Figure 2d). (P2$p_{3/2\text{-red}}$(P-S): 131.6 eV; P2$p_{3/2\text{-blue}}$(P-P): 129.9 eV; P2$p_{3/2\text{-green}}$(P-Li): 128.3 eV; S2$p_{3/2\text{-blue}}$(S-S): 164.1 eV; S2$p_{3/2\text{-red}}$(S-P): 163.1 eV; S2$p_{3/2\text{-red}}$(S-Li): 161.2 eV; Li1s_{red}(Li-S,Li-P): 55.0 eV; Li1s_{blue}(base line).) (d) The molecular models of the interaction between phosphorene and Li_2S_8, Li_2S_4, Li_2S_2, and Li_2S calculated *via* first-principles. The numbers (top line) represent the binding energies in each case. The middle and bottom line show the cross-section and top views, respectively.

Staircase potential electrochemical impedance spectroscopy [31] was employed to investigate the electrochemical reaction kinetics. The Nyquist plots of the electrochemical impedance spectra (**Figures 4a-c**) were recorded at the potentials of (A), (B) and (C) corresponding to **Figure 2a**. As shown in **Figures 4d-f**, the impedance spectra can be modelled with an equivalent circuit consisting of an ohmic resistance of the electrolyte and cell components (R_0) in series with one or more R//CPE elements (R and CPE connected in parallel) as well as a Warburg element (W_s).[32,33] A CPE was selected instead of a capacitor because of the non-ideal behavior of the system, reflected as suppressed semicircles in the Nyquist plots.

At OCV in **Figure 4a**, the value of ohmic resistance R_0 is 25-30 Ω for the both cells, indicating that the cells have been properly fabricated and tested in the same condition. However, the cell using the conventional separator has only one semicircle, whereas the cell using the phosphorene-modified separator has one more small semicircle at middle frequency region. Their equivalent circuits indicate that both of them have charge-transfer resistance at sulfur cathode R_1, while the P-modified cell has an interface contact resistance between phosphorene layer and cathode electrode R_2 resulting in the second semicircle. At 2.1 V in **Figure 4b**, both of the two cells have two semicircles related to the charge-transfer resistance at the cathode R_1, and the interface contact resistance between soluble polysulfides and cathode electrode R_2, respectively. Both of the R_1 and R_2 from the cell with conventional separator are larger than those in the phosphorene-modified cell. Discharged to 1.7 V in **Figures 4c**, the second semicircle in the cell with conventional separator increases dramatically, because the polysulfides adsorbed on the separator convert to solid lithium sulfide, leading to a larger interface contact resistance. In addition, for the case of the cell with conventional separator, an additional semicircle presents between R_1//CPE_1 and R_2//CPE_2, attributed to the immigration of polysulfides onto the anode side (R'_1//CPE'_1).

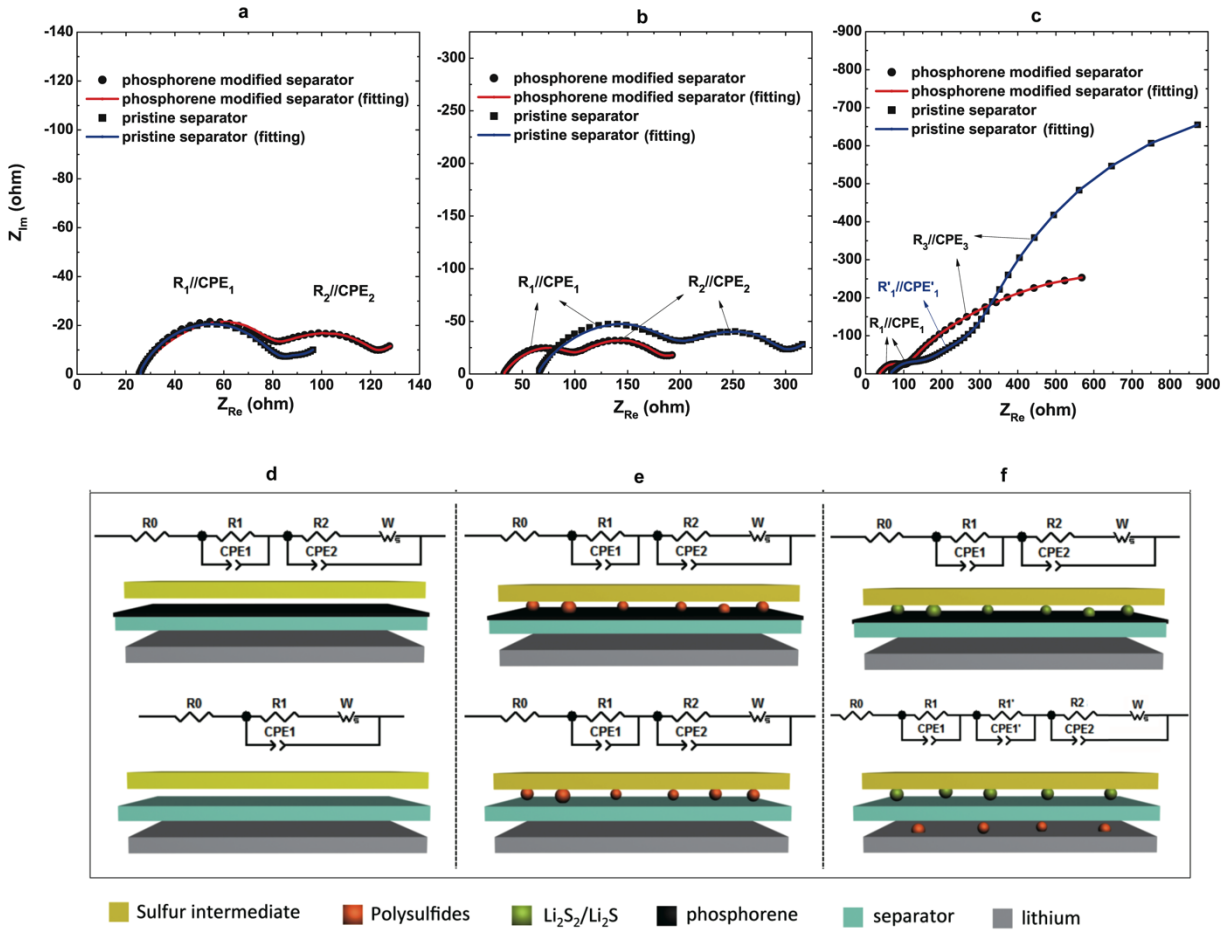

Figure 4. The electrochemical impedance spectra of the Li-S cells using phosphorene-modified and conventional separators, recorded at potentials (a) 2.42 V, (b) 2.1 V and (c) 1.7 V, respectively, corresponding to the potentials of (A), (B) and (C) in Figure 2a. (d-f) Equivalent circuits of the Li-S cells using phosphorene-modified (up) and conventional separator (down). (d), (e) and (f) are corresponding to (a), (b) and (c), respectively.

The effect of the phosphorene-modified separator on the electrochemical performance of a Li-S battery is reported in **Figure 5** and compared to a reference cell using a conventional separator and graphene-coated separator, prepared by replacing phosphorene with graphene (same loading). The first galvanostatic discharge–charge curves of the Li–S battery with the different separators at a current density of 0.4 A g^{-1} are shown in **Figure 5a**. The three cells show typical voltage profiles with two main discharge plateaus at around 2.3 V and 2.0 V, attributed to the reactions from solid S_8 to soluble Li_2S_x, and then to solid Li_2S, respectively. The beneficial effect of both coatings is particularly evident on the longer discharge plateau at ~2.0 V then that in the cell with conventional separator. It indicates that the modified separator inhibits the diffusion of polysulfides to the anode side, and reactivate the polysulfides

active. The initial discharge capacity of the phosphorene-modified cell can reach up to 930 mAh g^{-1}, which is 80 mAh g^{-1} higher than the graphene-modified cell, due to the stronger interaction of phosphorene for trapping the sulfur species. In addition, lithium ion can insert/extract into the phospnorene interlayers in the potential range of 1.7-2.6 V (**Figure S7**, Supplementary Information), contributing to an extra capacity. Moreover, for charging process, this Li^+ extraction reaction from phosphorene contributes to a lower overpotential than the other two cells. **Figure 5b** shows the cycling stability of the cells using the different separators. Comparing to the rapid capacity decay to ~300 mAh g^{-1} within 40 cycles of the cell using the conventional separator, the phosphorene-modified cell exhibits a capacity of 800 mAh g^{-1} after 100 cycles, corresponding to the retention rate of 86 %, much higher than the graphene-modified cell (66 % retention). The high rate cycling performance of the phosphorene-modified cell was further studied in **Figures 5c-d**. When the current rate was increased to 0.9 A g^{-1}, it could still deliver a reversible capacity of 820 mA h g^{-1}. Even at the very high rates of 1.8 A g^{-1} and 3.5 A g^{-1}, the electrode retained a specific capacity of 725 mA h g^{-1} (77 %) and 623 mA h g^{-1} (66 %), respectively.

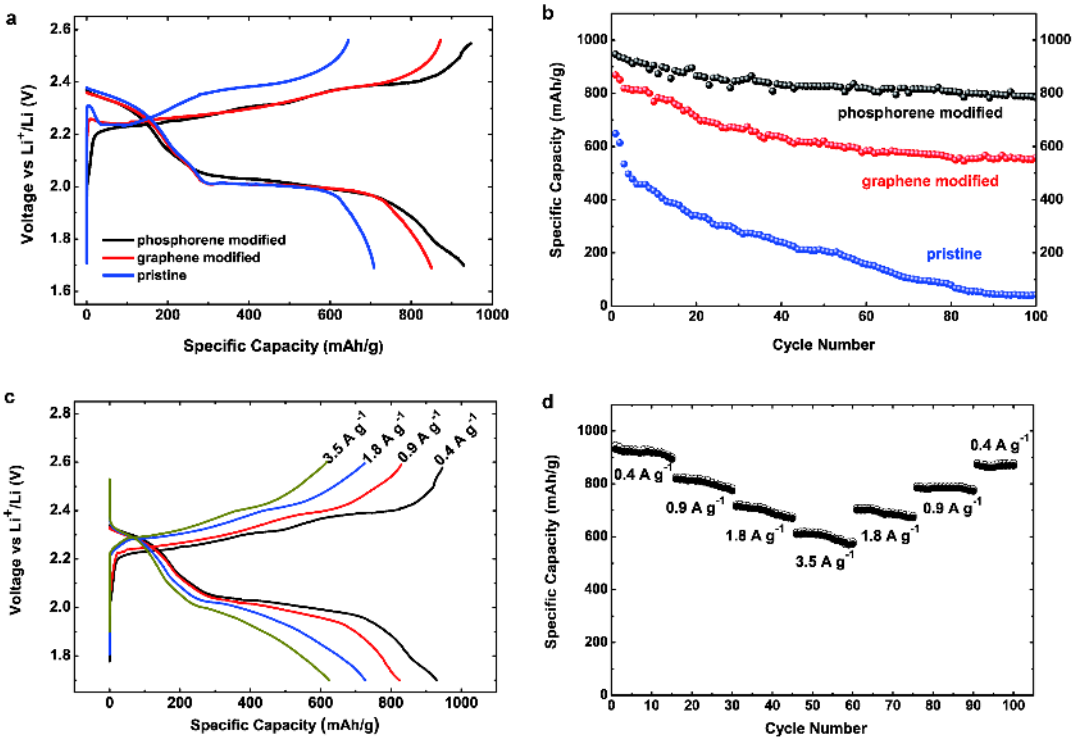

Figure 5. (a) First galvanostatic discharge–charge curves of the Li–S battery with phosphorene-modified, graphene-modified and conventional separators, respectively, at a current density of 0.4 A g^{-1}. (b) Reversible lithiation capacity and Coulombic efficiency for the first 100 galvanostatic cycles of the three Li–S cells, between 2.6 and 1.7 V at a current density of 0.4 A g^{-1}. (c) Galvanostatic discharge–charge curves of the Li–S cell with the phosphorene-modified separator, at different current densities (from 0.4

to 3.5 A g^{-1}). (d) Specific capacities of the Li–S cell with 5% phosphorene and phosphorene-modified separator, cycled at various rates.

In summary, a uniform 2D phosphorene layer, with high electron conductivity and ultrahigh Li diffusivity, was introduced on to a commercial polypropylene separator to trap and activate the soluble polysulfides in Li-S batteries. With such a functional composite separator, much increased specific capacity and improved cyclability are achieved for the sulfur electrode with a high sulfur content of 80%. This rational design was proposed based on the investigation of the polysulfides accommodated in the separator. The large surface area of the conducting coating, as well as the strong bonding with both of Li and S atoms, increased the utilization of the polysulfides accommodated in the separator. We showed that the Li–S battery performance was significantly improved with this conducting layer on the separators, indicating that phosphorene can open new avenues to improve the performance of Li–S batteries.

Experimental Section

Phosphorene (or graphene) coated separator: A phosphorene (or graphene) coated separator was fabricated by a vacuum-filtration. Typically, phosphorene was prepared by a liquid-phase exfoliation method[23]. Black phosphorus was dispersed in N-methyl-2-pyrrolidone (NMP) at a concentration of 0.1 mg ml^{-1} and sonicated in a sonic bath (Branson 5210 Ultrasonic) for 10 h. The resultaning dispersion of phosphorene was centrifuged using a Fisher Scientific accuSpin 400 centrifuge for 30 min at 3000 r.p.m. to remove sediment and obtain the supernatant. The suspension was mixed with 8 wt% polyvinylidene fluoride (PVDF) and subsequently vacuum filtered using a Celgard polyethylene separator (25 μm thick), followed by fully drying at 60 °C for 8 h. Finally, the dried phosphorene coated separator was punched into a disk with a diameter of 5/8 inch for assembling cells. The graphene coated separator was prepared following the above-mentioned process.

Sulfur cathode preparation

The sulfur cathode was prepared by conventional slurry coating. The slurry was prepared by mixing commercial sulfur powder, Super P, and PVDF with a mass ratio of 8:1:1 in an NMP solution overnight. The slurry was spread on the carbon coated aluminum substrate (MTI) by a doctor blade (20 milli-inch) and dried in a vacuum oven at 50 °C for 6 h. The sulfur mass loading in the cathode is 1.5–2 mg cm^{-2}.

Li-S prototype cell for *in situ* Raman

In situ Raman was performed using a transparent pouch cell, in which the cathode was punched a circular hole in the center with a diameter of 1/20 inch, so that laser was employed to detect Raman spectra of the surface on the separator. The cathode, modified separator, and lithium metal were packaged into the pouch cell. The aluminum strip and copper strip were connected to the cathode and lithium metal as two-electrode system connected to a VMP3 potentiostat (Bio-logic) for cell discharge/charge. The electrolyte (lithium bis(trifluoromethanesulfonyl)imide (1 M) in tetraethylene glycol dimethyl ether, ~50 μL) was injected into the cell. The fabricated cell was put on the stage of a Raman spectrophotometer (Horiba Jobin Yvon Raman equipped with a 532 nm laser) with the circular hole facing the laser for *in situ* characterization.

Electrochemistry

To evaluate the electrochemical performance of the modified separator, 2023 type coin cells (MTI) were assembled using lithium metal as the counter/reference electrode. The electrolyte was a freshly prepared solution of lithium bis(tri-fluoromethanesulfonyl)imide (LiTFSI) (1 M) in 1 : 1 v/v 1,2-dimethoxyethane and 1,3-dioxolane (DOL) containing $LiNO_3$ (1 wt%). 2032-type coin cells were assembled in an

argon-filled glove box and galvanostatic cycling of cells was carried out using an Arbin battery tester. Electrochemical impedance spectroscopy data were obtained with a VMP3 potentiostat (Bio-logic) from 200 KHz to 100 mHz with an AC voltage amplitude of 10 mV at the various voltages of the cells with the Li metal foil as both auxiliary and reference electrodes. Classic SPEIS was measured by a VMP3 electrochemical measurement system (Bio-logic). The frequency range of SPEIS was from 100 kHz to 0.1 Hz, and the potential sweep was from open circuit potential to 1.5 V. SPEIS involved the imposition of a 5 mV amplitude sine-wave. The potential step was 10 mV. At each frequency, impedance measurements were collected five times and the average impedance of those five measurements was recorded.

Acknowledgements

This work was supported by the Department of Energy, Office of Basic Energy Sciences, Division of Materials Sciences and Engineering, under contract DE-AC02-76SF00515.

Author contributions

Y.C. and J.S. conceived and designed the experiments. J.S. performed sample preparation, Raman, XPS, TEM and SEM characterization, and electrochemical measurements. J.S and M.P. performed the electrochemical measurements. J.S., Y.S., M.P. and Y.C. co-wrote the paper. All authors discussed the results and commented on the manuscript.

Additional information

Competing financial interests: The authors declare no competing financial interests.

References

[1] N. Li, Z. Weng, Y. Wang, F. Li, H.-M. Cheng, H. Zhou, *Energy Environ. Sci.* **2014**, *7*, 3307.

[2] P. G. Bruce, S. a. Freunberger, L. J. Hardwick, J.-M. Tarascon, *Nat. Mater.* **2011**, *11*, 172.

[3] D. Bresser, S. Passerini, B. Scrosati, *Chem. Commun.* **2013**, *49*, 10545.

[4] J. Shim, K. a. Striebel, E. J. Cairns, *J. Electrochem. Soc.* **2002**, *149*, A1321.

[5] Y. V. Mikhaylik, J. R. Akridge, *J. Electrochem. Soc.* **2004**, *151*, A1969.

[6] H. Yao, G. Zheng, P.-C. Hsu, D. Kong, J. J. Cha, W. Li, Z. W. Seh, M. T. McDowell, K. Yan, Z. Liang, V. K. Narasimhan, Y. Cui, *Nat. Commun.* **2014**, *5*, 3943.

[7] G. Zhou, S. Pei, L. Li, D.-W. Wang, S. Wang, K. Huang, L.-C. Yin, F. Li, H.-M. Cheng, *Adv. Mater.* **2014**, *26*, 625.

[8] L. Xiao, Y. Cao, J. Xiao, B. Schwenzer, M. H. Engelhard, L. V. Saraf, Z. Nie, G. J. Exarhos, J. Liu, *Adv. Mater.* **2012**, *24*, 1176.

[9] Y. Yang, G. Zheng, Y. Cui, *Chem. Soc. Rev.* **2013**, *42*, 3018.

[10] Z. Wei Seh, W. Li, J. J. Cha, G. Zheng, Y. Yang, M. T. McDowell, P.-C. Hsu, Y. Cui, *Nat. Commun.* **2013**, *4*, 1331.

[11] X. Ji, K. T. Lee, L. F. Nazar, *Nat. Mater.* **2009**, *8*, 500.

[12] Z. W. Seh, H. Wang, N. Liu, G. Zheng, W. Li, H. Yao, Y. Cui, *Chem. Sci.* **2014**, *5*, 1396.

[13] G. Zheng, Q. Zhang, J. J. Cha, Y. Yang, W. Li, Z. W. Seh, Y. Cui, *Nano Lett.* **2013**, *13*, 1265.

[14] Q. Zhang, Y. Wang, Z. W. Seh, Z. Fu, R. Zhang, Y. Cui, *Nano Lett.* **2015**, *15*, 3780.

[15] X. Tao, J. Wang, Z. Ying, Q. Cai, G. Zheng, Y. Gan, H. Huang, Y. Xia, C. Liang, W. Zhang, Y. Cui, **2014**, *1*.

[16] Z. W. Seh, J. H. Yu, W. Li, P.-C. Hsu, H. Wang, Y. Sun, H. Yao, Q. Zhang, Y. Cui, *Nat. Commun.* **2014**, *5*, 5017.

[17] Y.-S. Su, A. Manthiram, *Nat. Commun.* **2012**, *3*, 1166.

[18] Y.-S. Su, A. Manthiram, *Chem. Commun.* **2012**, *48*, 8817.

[19] S. Chung, A. Manthiram, *J. Phys. Chem. Lett.* **2014**, *5*, 1978.

[20] X. Wang, Z. Wang, L. Chen, *J. Power Sources* **2013**, *242*, 65.

[21] X. Han, Y. Xu, X. Chen, Y.-C. Chen, N. Weadock, J. Wan, H. Zhu, Y. Liu, H. Li, G. Rubloff, C. Wang, L. Hu, *Nano Energy* **2013**, *2*, 1197.

[22] J. Sun, G. Zheng, H. W. Lee, N. Liu, H. Wang, H. Yao, W. Yang, Y. Cui, *Nano Lett.* **2014**, *14*, 4573.

[23] J. Sun, H.-W. Lee, M. Pasta, H. Yuan, G. Zheng, Y. Sun, Y. Li, Y. Cui, *Nat. Nanotechnol.* **2015**, DOI 10.1038/nnano.2015.194.

[24] H. Yuan, X. Liu, F. Afshinmanesh, W. Li, G. Xu, J. Sun, B. Lian, A. G. Curto, G. Ye, Y. Hikita, Z. Shen, S.-C. Zhang, X. Chen, M. Brongersma, H. Y. Hwang, Y. Cui, *Nat. Nanotechnol.* **2015**, *10*, 1.

[25] W. Li, Y. Yang, G. Zhang, Y.-W. Zhang, *Nano Lett.* **2015**, *15*, 1691.

[26] Y.-R. Luo, *Comprehensive Handbook of Chemical Bond Energies*, CRC Press, Boca Raton, FL, **2007**.

[27] H. Yao, K. Yan, W. Li, G. Zheng, D. Kong, Z. W. Seh, V. K. Narasimhan, Z. Liang, Y. Cui, *Energy Environ. Sci.* **2014**, *7*, 3381.

[28] M. Hagen, P. Schiffels, M. Hammer, S. Dorfler, J. Tubke, M. J. Hoffmann, H. Althues, S. Kaskel, *J. Electrochem. Soc.* **2013**, *160*, A1205.

[29] Y. S. Su, Y. Fu, T. Cochell, a Manthiram, *Nat Commun* **2013**, *4*, 2985.

[30] B. Wang, S. M. Alhassan, S. T. Pantelides, *Phys. Rev. Appl.* **2014**, *2*, 1.

[31] H. Chen, Q. Zou, Z. Liang, H. Liu, Q. Li, Y. Lu, *Nat. Commun.* **2015**, *6*, 1.

[32] L. Yuan, X. Qiu, L. Chen, W. Zhu, *J. Power Sources* **2009**, *189*, 127.

[33] N. a. Cañas, K. Hirose, B. Pascucci, N. Wagner, K. A. Friedrich, R. Hiesgen, *Electrochim. Acta* **2013**, *97*, 42.